Turkish Journal of Electrical Engineering & Computer Sciences

http://journals.tubitak.gov.tr/elektrik/

Research Article

Turk J Elec Eng & Comp Sci
(2017) 25: 689 – 704

doi:10.3906/elk-1505-198

A power sharing control for microgrids based on extrapolation of injecting power and power-angle control

Suchart JANJORNMANIT*, Suttichai PREMRUDEEPREECHACHARN
Department of Electrical Engineering, Faculty of Engineering, Chiangmai University, Chiangmai, Thailand

Received: 23.05.2015 • **Accepted/Published Online:** 12.02.2016 • **Final Version:** 10.04.2017

Abstract: Droop controlled power sharing with an assumption that the value of line impedance is unavailable has been proven to have limitations; the power sharing is problematic in systems with significantly resistive lines. Furthermore, when the droop is applied in the islanding mode of operation of a microgrid, the system is likely to become unstable. In this paper, the droop control is replaced by an analytical solution. The proposed approach of power sharing is power-angle control of distributed generators (DGs), such as voltage source converters, a type of DG with extrapolation of power injected to the connected bus. It is demonstrated that the power injection to the bus could be tracked within the DG's capacity autonomously. Simulation and experimental results demonstrate the validity of the approach and it is shown that the proposed approach is suitable for DGs with either inductive or resistive line impedance. Moreover, this method can be operated in complex networks, such as meshed networks.

Key words: Active and reactive power sharing, autonomous microgrid, power-angle control, distributed generation, extrapolation

1. Introduction

Decentralized and autonomous power generation is more and more becoming a viable option for electrical energy supply in remote areas or systems where a connection to the public electricity grid is not economical. The concept of the microgrid (MG), which relies mainly on parallel connected power electronic converters, plays an important role in maintaining the overall power balance by sharing the load in the network. The widely used solution for power sharing in MGs is the droop control technique. Applications of droop control with minimum communication between generators can be found in, e.g., [1–4]. Droop controlled systems without using additional communication wiring were presented in [5,6]. Despite its proliferation, the droop control strategy itself is proven to have technical limitations [7,8], one of them being the persisting residual deviation from the control set point, e.g., in frequency control in MGs. To eliminate the residual frequency deviation, angle droop control was proposed in [9–11]. However, the method proposed in [9–11] relies on GPS to synchronize the individual controllers and to adjust their power sharing.

It has also been found that droop controlled power sharing is especially problematic when applied to systems with significantly resistive line impedance [5,7,8,12,13]. To improve control precision in such a situation, the concept of virtual impedance was proposed and successfully demonstrated in [14,15]. The concept is based on droop control voltage reference modification, compensating for the effect of line impedance in power sharing. Despite introducing an improvement, this concept, by choosing the virtual impedance, requires a trade-off

*Correspondence: suchart@rmutl.ac.th

between power sharing and voltage frequency/magnitude regulation [8]. Nevertheless, the concept of virtual impedance already demonstrates the existence of a relationship between line impedance and how the power is shared among the generators in a MG.

The proposed analysis of power sharing is carried out by dividing the network into two elements: 1) the power generation unit and 2) the interconnection line connecting a distributed generator (DG) and common bus. In the power generation unit, the control of power into the network of a synchronous generator [16] is emulated, with the assumptions that the active power is generated depending on a phase angle difference between terminal and generating voltage, where the reactive power depends on a difference in magnitude of the two voltages.

To extrapolate the power flow through the interconnection line from the DG to the common bus, the power flow is analyzed by using a phasor diagram, which is then combined with the phasor diagram of the power generation unit. The resulting diagram can be used to calculate the absolute voltage and phase angle difference required from the generation unit in order to precisely supply the demanded powers, while at the same time maintaining the voltage magnitude at the bus at its intended value.

In this paper, the relationship is analyzed based on the assumption that the impedance of the line connecting DG and its connected bus is known. Although measurement of the line impedance is difficult, there are successful works on this problem [17,18] and its calculation and estimation can be found in [16]. Despite the analysis of this research focusing on VSC-based power generation units, the implementation is not limited to this class of DGs. Any generation technologies capable of adjusting their output voltage as described in this paper can be implemented in the presented technique.

2. Power sharing analysis

Figure 1 depicts a typical microgrid, with each DG connected to its bus directly or via its own line. The analysis is based on an assumption that each of the DGs needs to share the power provision while at the same time commonly regulate the voltage magnitude at the connected bus. Figure 2 shows the power delivery from the DG to its connected bus, and the analysis is divided into two parts: the generation unit and the interconnection line.

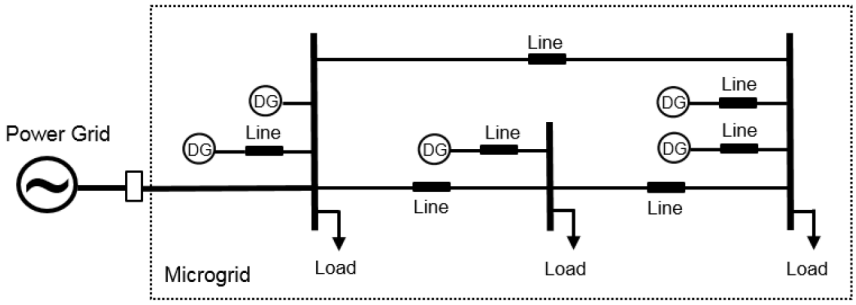

Figure 1. Typical microgrid.

2.1. Power generation by power-angle control

To generalize the analysis of the power generation of each DG, the phase of the DG's terminal voltage is used as the DG's reference phase. Each of the DGs acts like a synchronous generator [16] and the power delivery via an inductor to DG terminal is governed by Eqs. (1) and (2). Figure 3 shows a phasor diagram of the terminal voltage, V_t, the generating voltage, V_g, and the line current, I, in the DG.

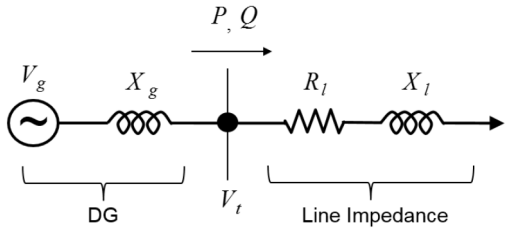

Figure 2. Power delivery from the DG to its connected bus via its own line.

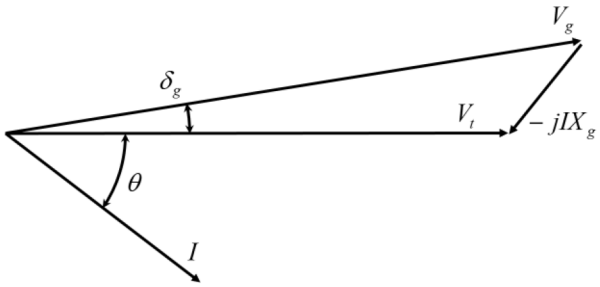

Figure 3. Phasor diagram of power generation at one of the DGs.

The active power, P, transferred to the DG terminal [16] can be calculated by:

$$P = \frac{|V_g| \cdot |V_t|}{X_g} \sin(\delta_g), \tag{1}$$

where δ_g is the angle difference between V_t and V_g, and X_g is the output inductance of the DG. In addition, the reactive power transferred, Q [16], can be calculated by:

$$Q = \frac{|V_t|}{X_g} \left(|V_g| \cos(\delta_g) - |V_t|\right). \tag{2}$$

Based on the assumption that δ_g is small, it can be interpreted from Eqs. (1) and (2) that an increase in δ_g causes a larger change in P than Q and Q is varied depending on the voltage magnitude difference between the terminal and generating voltage [7].

2.2. Power flow through interconnection line

Figure 4 shows the phasor diagram of V_t, I, and the voltage on the bus. The angle difference between V_t and V_{bus}, named δ_l, is varied depending on how the powers are transferred from the DG terminal to the bus via an interconnection line.

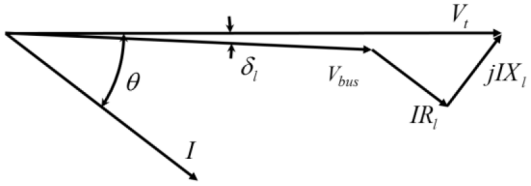

Figure 4. Phasor diagram of the feeding powers through interconnection line.

The active power delivered to the bus [7] is given by:

$$P = \frac{|V_t|}{R_l^2 + X_l^2} \left[R_l \left(|V_t| - |V_{bus}| \cos(\delta_l) \right) + X_l |V_{bus}| \sin(\delta_l) \right], \tag{3}$$

where R_l and X_l are the resistance and inductance of the line impedance. In addition, the reactive power delivered [7] is given by:

$$Q = \frac{|V_t|}{R_l^2 + X_l^2} \left[-R_l |V_{bus}| \sin(\delta_l) + X_l \left(|V_t| - |V_{bus}| \cos(\delta_l) \right) \right]. \tag{4}$$

2.3. Power sharing by droop control

In the general case, the droop adjusts its voltage and frequency linearly to output power [7], as illustrated in the following equations:

$$f - f_o = -k_p(P - P_o), \tag{5}$$

$$V - V_o = -k_q(Q - Q_o), \tag{6}$$

where f is output frequency, V is the output voltage, k_p and k_q are the droop gains, and the subscript o indicates its rated value. It can be interpreted from the equations that the frequency and voltage are changed linearly by the power from their rated values. When compared with the relation from Eqs. (1)–(4), the feeding power to the bus is actually nonlinear to voltage, whereas frequency adjusting of the droop is the determination to change the active power in steady-state operation. The relationship of voltage, frequency, and power is actually not straightforward as in the droop equations.

2.4. Extrapolation of injecting power

The preceding two phasor diagrams in Section 2.1 and 2.2 are combined in Figure 5. Based on the assumption that DGs need to share the power while commonly regulating the voltage magnitude at the bus, it can be assumed from the diagram that the magnitude of the voltage at the bus, $|V_{bus}|*$, is treated as a constant value to determine the required constraint operation of the DGs. The magnitude of line current and the angle of power factor, θ, can be measured at a DG terminal.

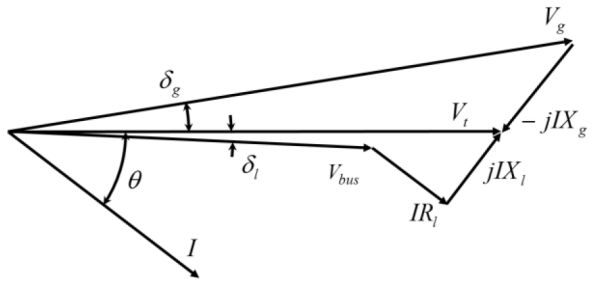

Figure 5. Phasor diagram of DG and interconnection line.

If the line impedance is known or at least can be estimated with sufficient accuracy, the angle difference between the DG terminal and the bus voltage can be calculated by:

$$\delta_l = \sin^{-1} \left(\frac{|I| \left(X_l \cos(\theta) - R_l \sin(\theta) \right)}{|V_{bus}|^*} \right), \tag{7}$$

and then the magnitude of DG terminal voltage can be calculated by:

$$|V_t| = |V_{bus}|^* \cos(\delta_l) + |I| \left(R_l \cos(\theta) + X_l \sin(\theta)\right). \tag{8}$$

Therefore, the angle difference between terminal and generating voltage, which is the control of active power generation, can be calculated by:

$$\delta_g = \tan^{-1}\left(\frac{|I| X_g \cos(\theta)}{|V_t| + |I| X_g \sin(\theta)}\right). \tag{9}$$

The magnitude of generating voltage can be calculated by:

$$|V_g| = \frac{|I| X_g \cos(\theta)}{\sin(\delta_g)}. \tag{10}$$

Thus, the magnitude difference between terminal and generating voltage, ΔV, which is the control of reactive power generation, is known and can be maintained.

2.5. Consideration of maximum output power limitation

DGs are limited by their maximum generation capacity. From Eq. (1), the maximum allowable active power, P_m, can be translated into a maximum angle difference between DG terminal and generating voltage, δ_{gm}, which can be calculated by:

$$\delta_{gm} \approx \sin^{-1}\left(\frac{P_m X_g}{\left(|V_{bus}|^*\right)^2}\right). \tag{11}$$

In addition, the maximum allowable reactive power, Q_m, is a maximum of the magnitude difference between DG terminal and generating voltage, ΔV_m. From Eq. (2), it can be expressed as:

$$\Delta V_m \approx \frac{Q_m X_g}{|V_{bus}|^*}. \tag{12}$$

3. Reference voltage generation

The analysis is based on the assumption that the load is balanced. Therefore, the terminal voltage and current sensing from one of the three phases is sufficient for performing the reference voltage generation. If the system is unbalanced all three lines need to be sensed and the proposed reference voltage generation may be formulated in the rotating d-q-0 coordinates. The reference voltage is generated by Eqs. (9) and (10), and it is revised every cycle or at least every few cycles; therefore, the terminal voltage zero phase angle detection (it can be PLL) is needed. To overcome the effect of inaccurate parameters, such as voltage tracking error and line impedance mismatch, a condition is needed. The condition is that if the changes of δ_g and V_g from the last cycle (or last update) are within a threshold, such as $\pm 5\%$ of δ_{gm} and ΔV_m, the power generation is locked by setting δ_g and V_g to the last cycle's (or last update's) values. In addition, as soon as the terminal voltage changes by $\pm 1\%$ of ΔV_m from the locking point, the power generation is unlocked.

The active power is limited to the DG's capacity by permitting P to be within zero and P_m, and when the active power is settled outside its limit, δ_g is forced to increase or decrease by a small amount of angle (use

$\pm 1\%$ of δ_{gm}). The reactive power is controlled by varying V_g in accordance with Eq. (10), and the reactive power is also controlled to be within zero and Q_m. When the reactive power is settled outside its capacity, V_g from Eq. (10) is changed to relax the reactive power sharing among the DGs. V_g is forced to increase or decrease by a small amount of voltage (use $\pm 1\%$ of ΔV_m). The flowchart of the reference generation is depicted in Figure 6. Figure 7 shows the VSC that uses the reference voltage generator.

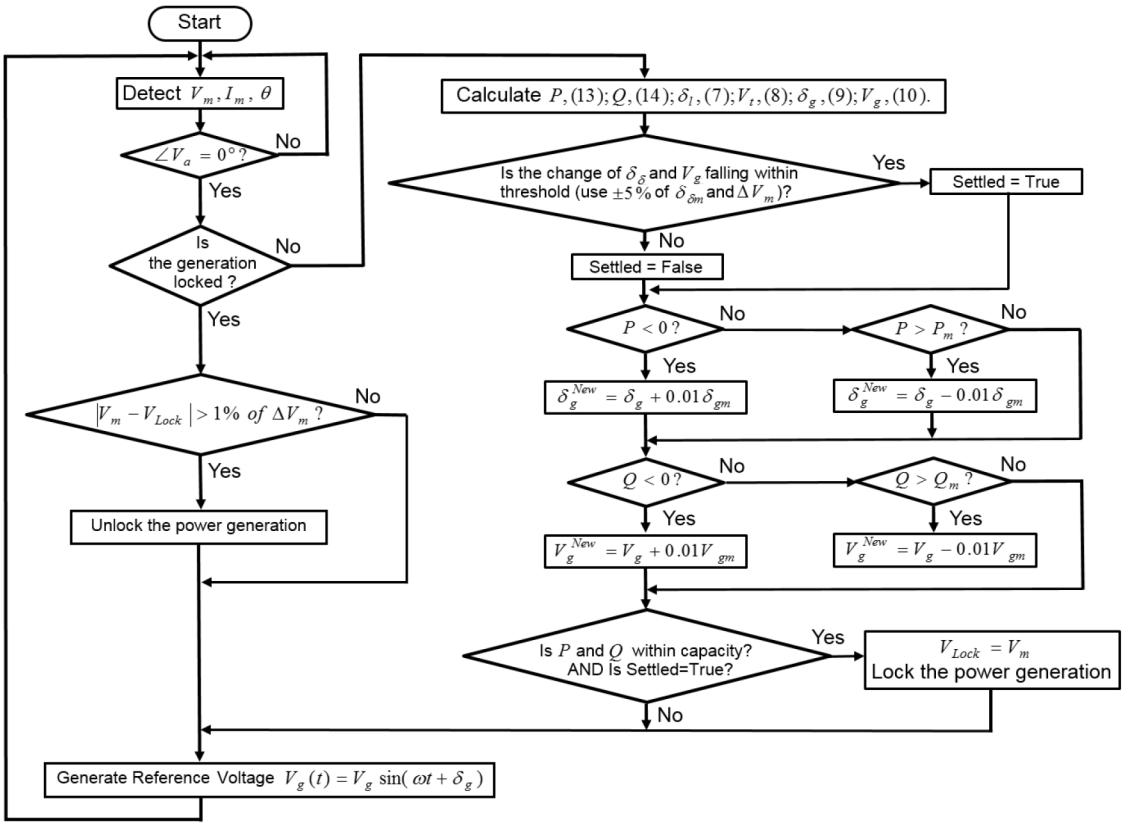

Figure 6. Flowchart of the reference voltage generator.

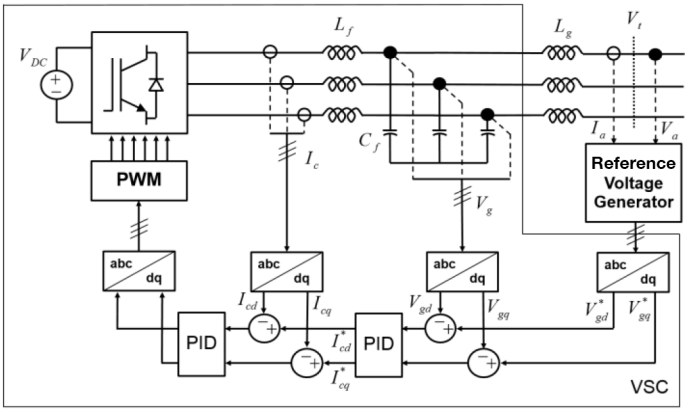

Figure 7. A VSC for use with the reference voltage generator.

The power is calculated at the end of voltage cycle by:

$$P = \frac{V_{\max} I_{\max} \cos(\theta)}{2}, \tag{13}$$

$$Q = \frac{V_{\max} I_{\max} \sin(\theta)}{2}, \tag{14}$$

where the subscript *max* indicates its peak value in the cycle.

4. Simulation study

The simulation is performed by MATLAB/Simulink. The operation of the network is regarded as the islanding microgrid. The system is a balanced 3-phase 380 V/50 Hz, and the reference voltage's frequency is a fixed 50 Hz. In each case of simulations, the system's parameters and the simulation results are indicated in the system diagram, and the results are in brackets. The results are the locked values when the system is in stable and steady-state power sharing. All values in the diagrams are per unit with base MVA of 1 MVA and base kV $_{LL}$ of 0.380.

4.1. System with VSC-type DG

The structure of the VSC is shown in Figure 8 and the Table gives parameters for the VSC. The simulation result for a system with the VSC-type DG is shown in Figure 9a. The values in brackets are the voltages and powers that have been locked due to the system reaching the stable and steady-state power sharing point. It is shown that the system is stable even though there is a voltage tracking error by the VSC, but for the sake of controllability, the error should be minimal.

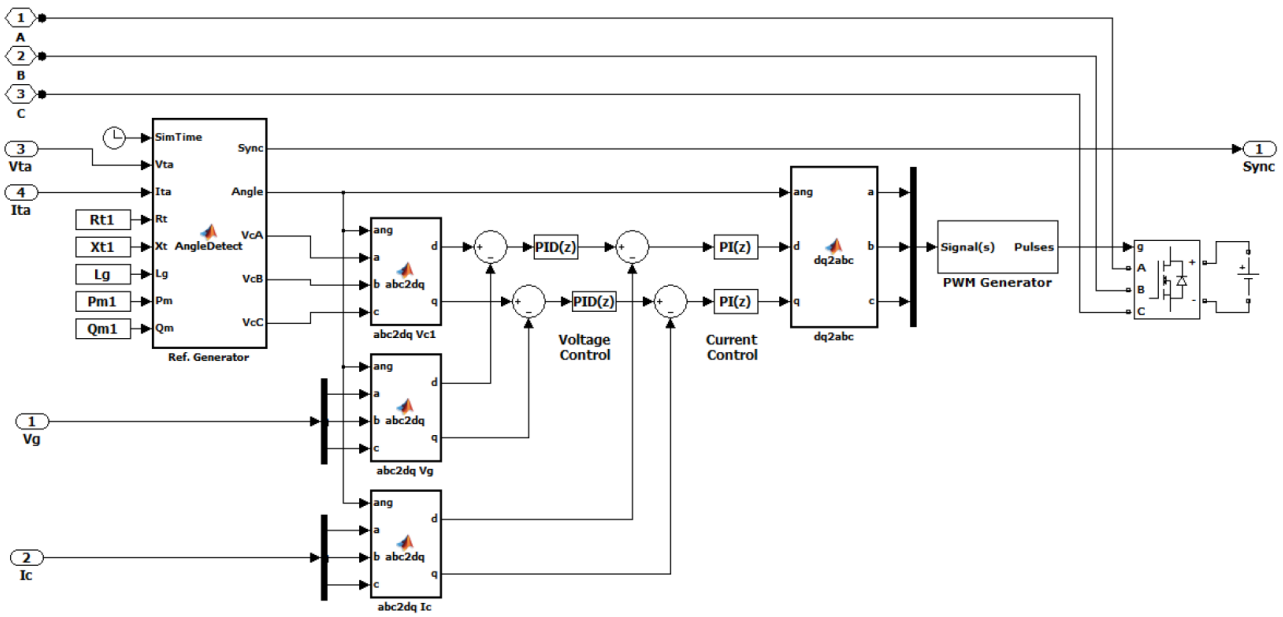

Figure 8. Structure of the VSC for MATLAB/Simulink simulation.

Table. Parameters for the VSC.

Item	Symbol	Value
PWM switching frequency	f_{sw}	10 kHz
Filter inductor	L_f	1.5 mH
Filter capacitor	C_f	3300 μF
DC link voltage	V_{DC}	700 V
Voltage P-control gain (d & q)	K_P	3000
Voltage I-control gain (d & q)	K_I	100
Voltage D-control gain (d & q)	K_D	10
Current P-control gain (d & q)	K_P	100
Current I-control gain (d & q)	K_I	10

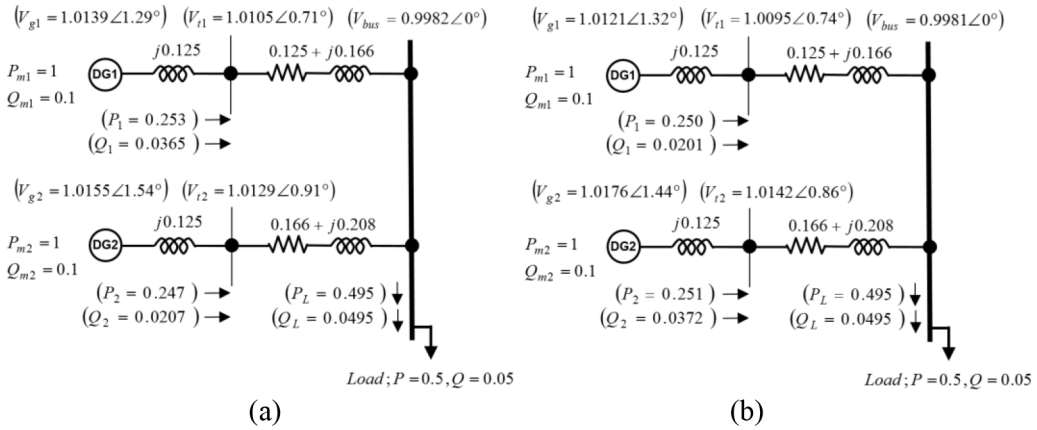

Figure 9. (a) Results of the system with the VSC-type DG, (b) results of the system with the controlled voltage source.

4.2. Perfect tracking, case study

In order to investigate the proposed analysis of power sharing without concern for the reference voltage tracking error, the VSC in Figure 7 is replaced by the 'Controlled Voltage Source' block in the 'SimPowerSystems' toolbox of MATLAB/Simulink. The voltage reference is fed directly to the block so that the output voltage is perfectly generated. The controlled voltage source used in the simulation is not used to solve the problem of the VSC, and there is no problem for the VSC to be used with the proposed method when the voltage tracking error is minimal. The use of the controlled voltage source in the simulation is merely implemented to show the effectiveness of the proposed method when there is no constraint over voltage tracking error. The same reference voltage generation is used in both the controlled voltage source and the VSC case study.

The results of the system with the controlled voltage source, which is considered to have no voltage tracking error, are given in Figure 9b; the results are slightly different from the case of the VSC-type DG (with minimal tracking error). This demonstrates that the condition of locking the power generation by checking the change of power is able to overcome the effect of voltage tracking error.

4.2.1. Effect of inaccurate line impedance

The simulation results of the system with inaccurate line impedance are shown in Figure 10. The value of line impedances used for calculation in Eqs. (7) and (8) for the reference voltage generation of DG1 is 0.166+j0.021 plus 5% error, and that of DG2 is 0.166+j0.208 minus 10% error. The power generations are locked as values

indicated in brackets; this means that even though the line impedances are not correct, the condition to lock the power generation by checking the change of power is also able to overcome the effect of inaccurate line impedance. For the sake of controllability, however, the inaccuracy should be minimal.

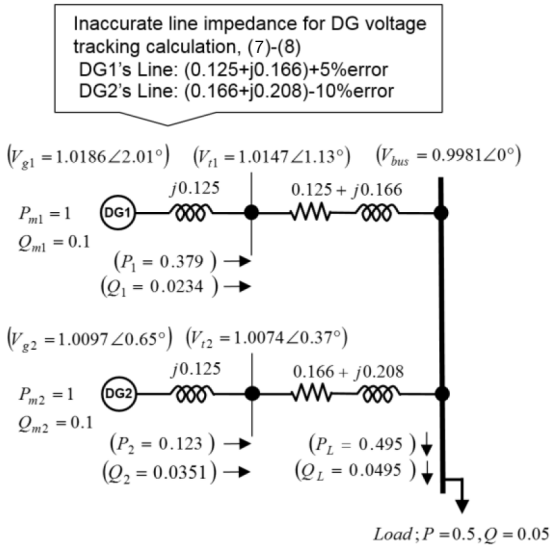

Figure 10. Results of the system with inaccurate line impedance.

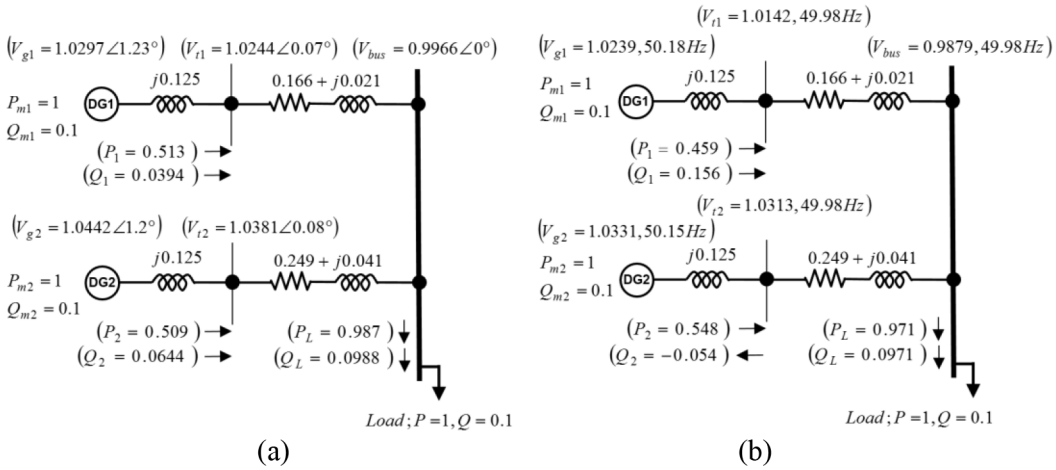

Figure 11. Results comparing between the proposed method and the droop in the same system: (a) results of the proposed method, (b) results of the droop.

4.2.2. System with resistive line

The simulation results of the system with resistive line are given in Figure 11a. The lines of DG1 and DG2 are resistive, whereas the previous cases are inductive. This means that the proposed approach is able to operate with either resistive or inductive line impedance.

4.2.3. Power sharing by droop control

To compare the performance of power sharing with the droop control in the same system of resistive lines, the power sharing by droop in Eqs. (5) and (6) is implemented and the simulation results of the droop are given in

Figure 11b. V in Eq. (6) is a generating voltage, V_g. Rated values in Eqs. (5) and (6) for both DG1 and DG2 are P_o = 1 MW, Q_o = 100 kVar, f_o = 50 Hz, and V_o = 390 V. V_o is increased from 380 V to compensate for voltage drop on the line and output inductor. Droop gains for both DG1 and DG2 are K_p = 1 Hz/1 MW and K_q = 3 V/100 kVar. As it is widely known that the performance of droop control depends largely on the value of droop gain, at this value of gain, the power sharing is stable, but there are three main problems noticed from the results. The first problem is that the frequency deviates from its rated value, 50 Hz. The second problem is that the reactive power of DG2 is negative; in other words, DG2 acts like a load. This means that there is an exchange of power between DG1 and DG2 and it decreases the performance of power generation. Another problem is that the reactive power of DG1 is over its capacity; the droop control is unable to force the power to be within its capacity. When comparing the results between the proposed method in Figure 11a and the droop control in Figure 11b, there is no negative Q and it operates at a fixed system frequency when the system is controlled by the proposed approach. The results validate the superiority of the proposed method over the droop control.

4.2.4. Effect of changing load

Figure 12 shows system for simulation of changing load. The load begins with P = 0.75, Q = 0.05, and the locked values before the load changing are shown in Figure 12a. At 1.5 s the load is step changed to P = 1.25, Q = 0.15 and the simulation result during load changing is given in Figure 13. The simulation results of locked values after the load changing are given in Figure 12b.

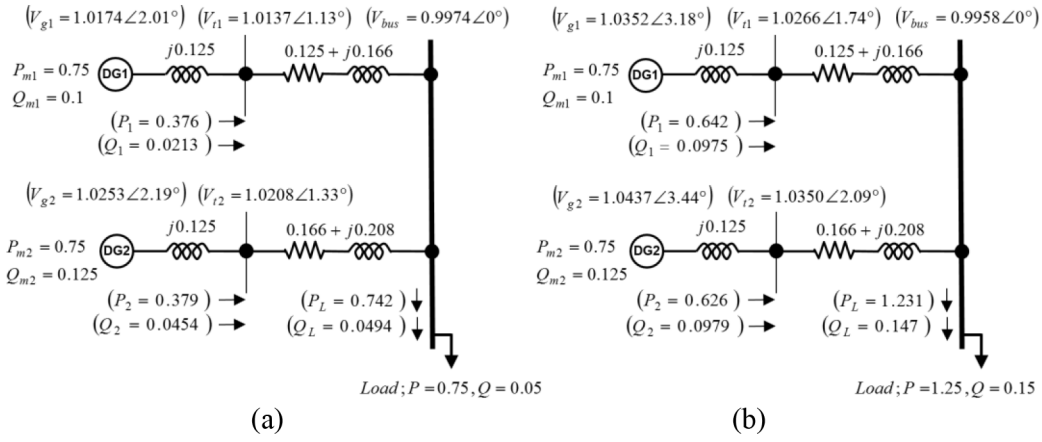

Figure 12. Results of the system with step change of load: (a) locked values before changing, (b) locked values after changing.

The values of locked powers and voltages cannot be predetermined; the power the DG needs to share depends on $|V_{bus}|$. A different $|V_{bus}|$is different power sharing; $|V_{bus}|$is changing up and down while the proposed approach is finding the locking point. It depends on time and the response of the system that the locking point is found at any given value of $|V_{bus}|$. Even though the locking point cannot be predetermined, the proposed approach is able to find it when sufficient conditions are met. The ratio and how the power is shared are governed by Eqs. (3) and (4).

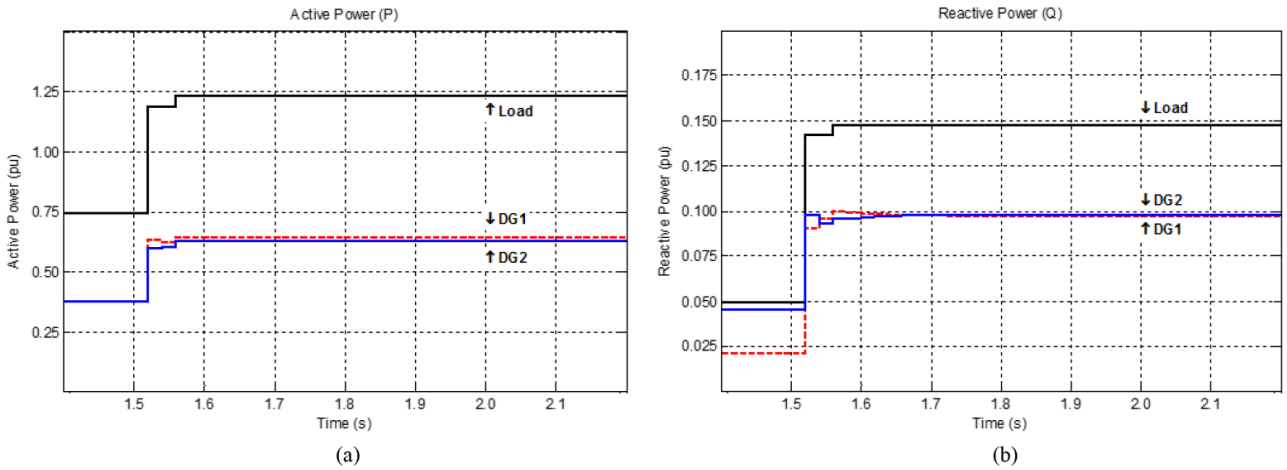

Figure 13. Results of the system with step change of load: (a) result of active power, (b) result of reactive power.

4.2.5. Consideration of type of network

The simulation results of four DGs parallel connected to supply a common load are shown in Figure 14. The ratio and how the power is shared are complex. The feeding of P and Q through line depends on Eqs. (3) and (4), and both equations use the same variables, $|V_t|$, $|V_{bus}|$, and δ_l. It can be interpreted from the equations that line impedance decides the relationship between P and Q of its DG, and the values of P and Q depend on $|V_t|$ and δ_l, whereas the only common value between the DGs that are connected to the same bus is $|V_{bus}|$. It decides the relationship of power sharing among DGs in the same bus.

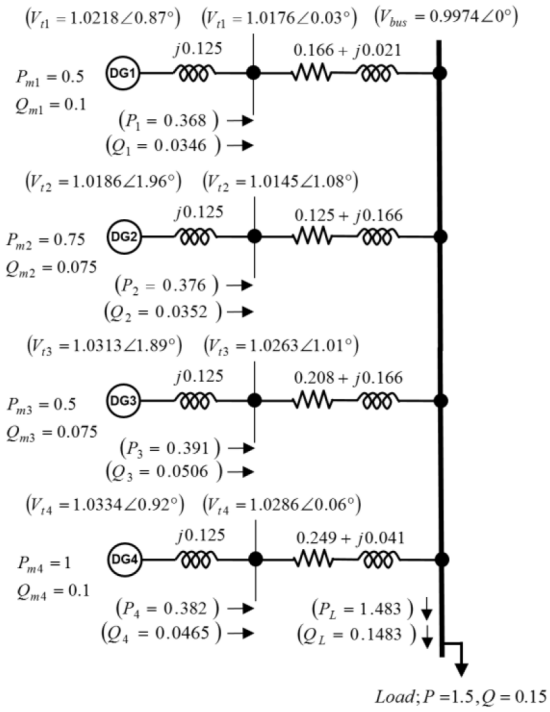

Figure 14. Results of 4 DGs parallel connected to supply a common load.

The simulation results of a network with two buses are shown in Figure 15. The simulation results of a three-bus meshed network are shown in Figure 16. DG1 in Figures 15 and 16 has no line; this is the determination to demonstrate that the DG is directly connected to the bus. The power sharing between two buses via a line also depends on Eqs. (3) and (4), and in this case $|V_t|$ is replaced by another $|V_{bus}|$. The relationship of power sharing is the same as that of the feeding of power from DG to the bus via a line.

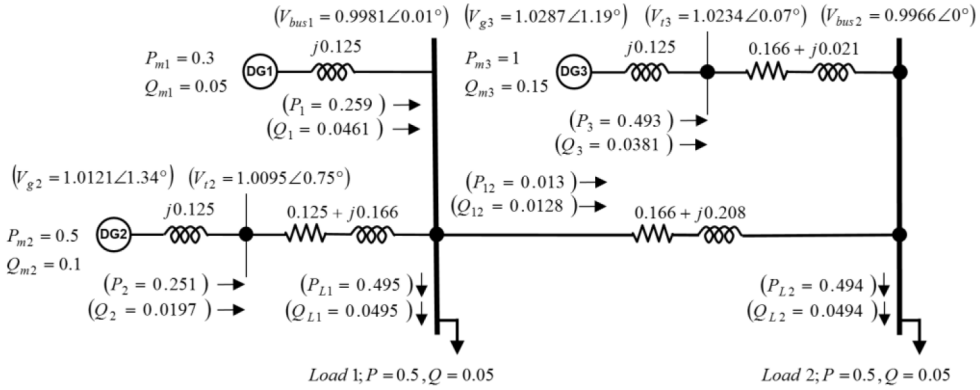

Figure 15. Results of a network with two buses.

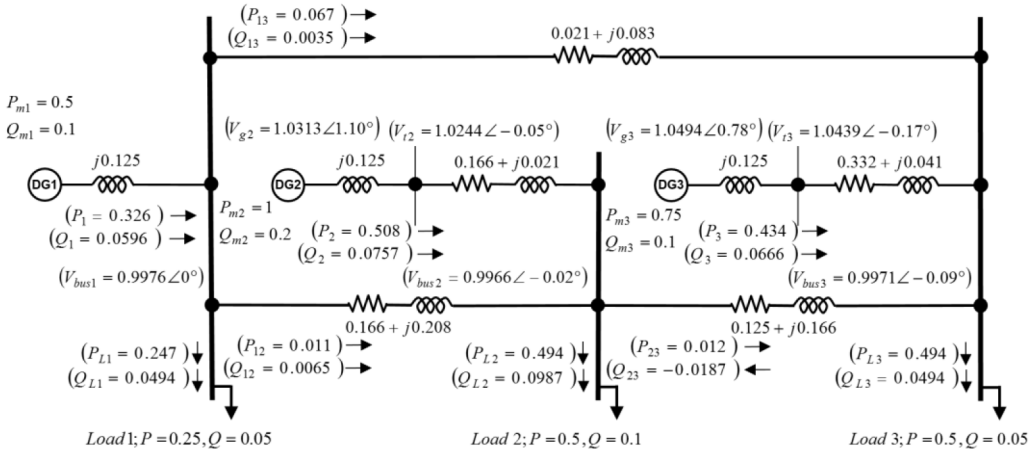

Figure 16. Results of three-bus meshed network.

5. Experimental results

The proposed approach is implemented in a down-scale single-phase 220 V/50 Hz system. Figure 17 shows the configuration of the system of two DGs; all parameters are included in the figure. To simplify the operation of the V_g control, V_g in the experiment is controlled by a direct voltage-PWM control loop. The control function of both DGs is operated by a single dSPACE system, but modules of the proposed power sharing control for each DG are separated. The dSPACE is operated in the following steps.

Step 1 starts by tracking the new power sharing point by sustaining the output reference voltage with fixed magnitude and phase.

Step 2 detects the phase angle and peak of waveforms of terminal voltage and current of both DGs. This may take a few cycles to gain accurate values.

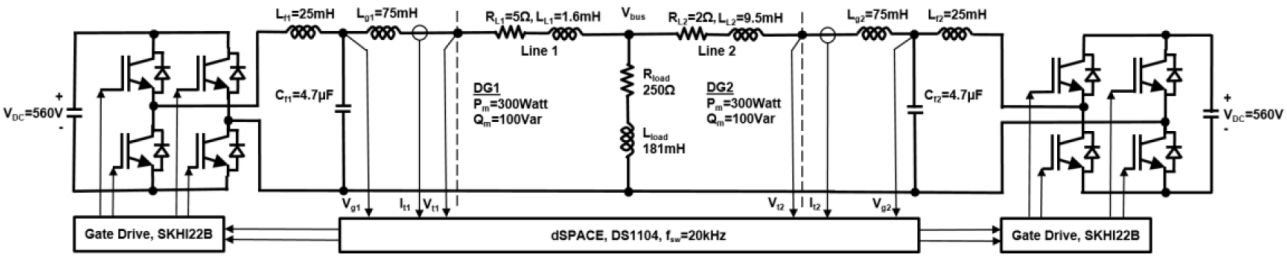

Figure 17. Configuration of the experimental system.

Step 3 calculates the new power sharing point by the proposed approach and updates the new sharing point by repeating from Step 1.

Figure 18 shows the test bench of the implemented system during its operation. There are problems related to the implementation of the VSC-type DG. The recommendation is given as follows for implementation of the proposed approach. If there is a noisy environment, voltage fluctuation by the controlling of VSC, and inaccuracy of the phase angle and peak detection, then the adjustment of power sharing by Eqs. (9) and (10) may not be smooth and desirable. These problems cause sudden changing of V_g and δ_g in Eqs. (9) and (10), and then the system may not be stable. In order to mitigate those effects on power sharing, it is recommended that prior to updating the values of V_g and δ_g, the sudden changing should be filtered out by:

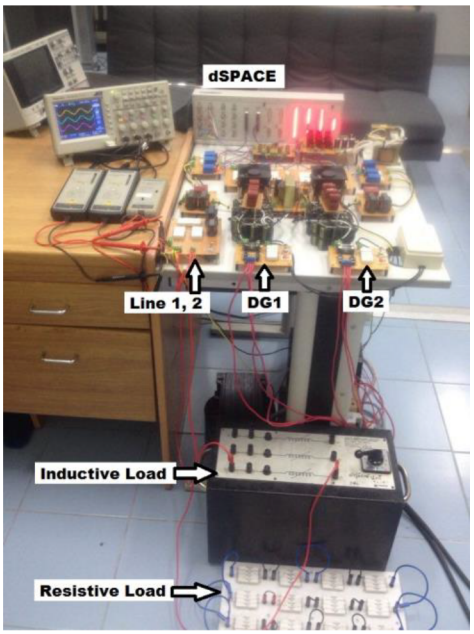

Figure 18. Test bench of the experiment during operation.

$$\delta_g^N = \delta_g^{i-1} + f_d\left(\delta_g^i - \delta_g^{i-1}\right), \tag{15}$$

$$V_g^N = V_g^{i-1} + f_d\left(V_g^i - V_g^{i-1}\right), \tag{16}$$

where superscript i indicates the consecutive cycle (or update) of the calculation of Eqs. (9) and (10), and superscript N indicates the actual new updated values of V_g and δ_g. The damping multiplier, f_d, can be

calculated by:

$$f_d = C_d \frac{\left(\Delta V_m - \left(V_g^i - V_g^{i-1}\right)\right)}{\Delta V_m}. \tag{17}$$

C_d is a damping coefficient and the value is between 0 and 1. For the system without any concerns about those effects, such as in the simulation study, C_d can be 1. A lower value of C_d signifies more mitigation of the effects on power sharing, but its response would be slower. In the experiment, it has been found that C_d= 0.2 is the optimal value in test conditions. If the change of V_g, $\left(V_g^i - V_g^{i-1}\right)$, in Eq. (17) is more than ΔV_m, then it is limited to ΔV_m; this means that the values of V_g and δ_g should not be changed immediately when there is a sudden changing of V_g from its calculation in Eq. (10). In addition, the multiplication of the damping multiplier, f_d, is not necessary for the system without any concern about those problems, such as in the simulation study.

During the experiment, the power of each DG is changing up and down a little bit, but the overall system is stable and the sum of the power of the two DGs is the sum of the load, lines, and losses. Figure 19 shows the results of voltage waveforms during its operation. Figure 20 shows the results of the experiment per unit, with base kVA = 0.3 and base kV = 0.22. The parameters in the diagram are the same values as in Figure 17. As mentioned above, during the experiment the power of each DG is changing up and down a little bit due to the effects of noises, voltage tracking error, and inaccuracy of the detections; therefore, all the results in brackets are average values.

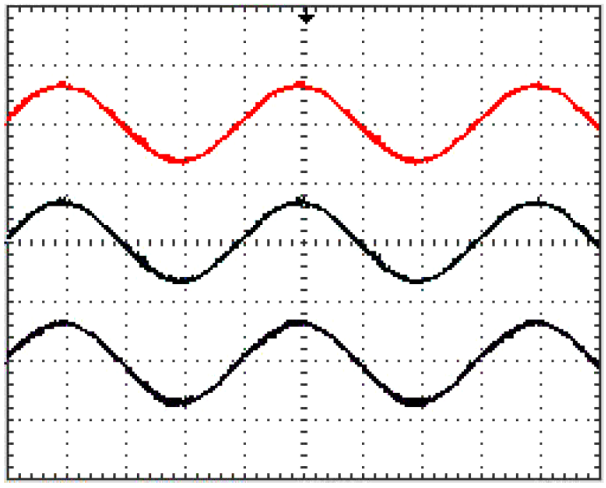

Figure 19. Result of voltage waveforms: upper waveform is V_{bus}, middle waveform is V_t of DG1, lower waveform is V_t of DG2. Vertical scale is 500 V/Div, time scale is 5 ms/Div.

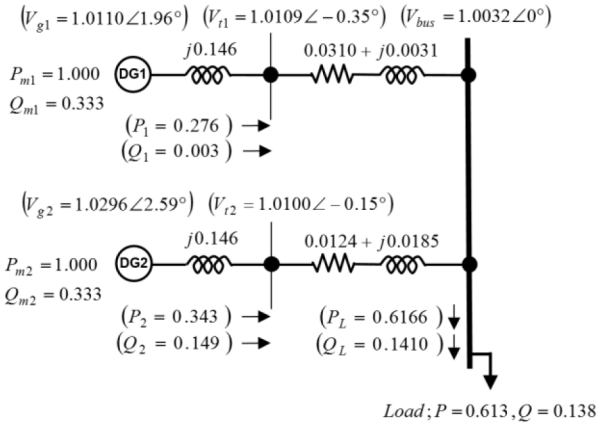

Figure 20. The experimental results.

6. Conclusion

This article proposes a novel methodology to control active and reactive power sharing in a microgrid. The proposed technique is based on the extrapolation of injected power within its capacity from the DG to the connected bus via an interconnection line. The presented technique is able to operate autonomously in islanding mode and in the DG with either inductive or resistive lines. The simulation and experimental results also show

that the proposed approach is suitable for most types of network, and the stable and steady-state power sharing point is reachable even in imperfect conditions, such as when conditions include voltage tracking error, inaccurate line impedance, and sudden load changing.

Acknowledgments

This project was performed partly under the National Research University Project, Office of the Higher Education Commission, Thailand and Chiang Mai University. The authors would like to thank the National Science and Technology Development Agency and Rajamangala University of Technology Lanna for a scholarship and support of the study.

References

[1] Katiraei F, Iravani MR. Power management strategies for a microgrid with multiple distributed generation units. IEEE T Power Syst 2006; 21: 1821-1831.

[2] Prodanovic M, Green TC. High-quality power generation through distributed control of a power park microgrid. IEEE T Ind Electron 2006; 53: 1471-1482.

[3] Marwali MN, Jung JW, Keyhani A. Control of distributed generation systems—Part II: Load sharing control. IEEE T Power Electron 2004; 19: 1551-1561.

[4] Mehrizi-Sani A, Iravani R. Potential function based control of a microgrid in islanded and grid-connected modes. IEEE T Power Syst 2010; 25: 1883-1891.

[5] Guerrero JM, Matas J, Vicuña LG, Castilla M, Miret J. Wireless-control strategy for parallel operation of distributed generation inverters. IEEE T Ind Electron 2006; 53: 1461-1470.

[6] Brabandere KD, Bolsens B, Keybus JVD, Woyte A, Driesen J, Belmans R. A voltage and frequency droop control method for parallel inverters. IEEE T Power Electron 2007; 22: 1107-1115.

[7] Rocabert J, Luna A, Blaabjerg F, Rodriguez P. Control of power converters in AC microgrids. IEEE T Power Electron 2012; 27: 4734-4749.

[8] Guerrero JM, Chandorkar J, Lee T, Loh PC. Advanced control architectures for intelligent microgrids—Part I: Decentralized and hierarchical control. IEEE T Ind Electron 2013; 60: 1254-1262.

[9] Majumder R, Ghosh A, Ledwich G, Zare F. Angle droop versus frequency droop in a voltage source converter based autonomous microgrid. In: Proceedings of the IEEE PES General Meeting; 2009. New York, NY, USA: IEEE. pp. 1-8.

[10] Majumder R, Chaudhuri B, Ghosh A, Majumder R, Ledwich G, Zare F. Improvement of stability and load sharing in an autonomous microgrid using supplementary droop control loop. IEEE T Power Syst 2010; 25: 796-808.

[11] Majumder R, Ghosh A, Ledwich G, and Zare F. Load sharing and power quality enhanced operation of a distributed microgrid. IET Renew Power Gen 2009; 3: 109-119.

[12] Tabatabaee S, Karshenas HR, Bakhshai A, Jain P. Investigation of droop characteristics and X/R ratio on small-signal stability of autonomous microgrid. In: Proceedings of the 2nd PEDSTC Conference; 2011. New York, NY, USA: IEEE. pp. 223-228.

[13] Peng FZ, Li YW, Tolbert LM. Control and protection of power electronics interfaced distributed generation systems in a customer-driven microgrid. In: Proceedings of the IEEE Power Energy Society General Meeting; 2009. New York, NY, USA: IEEE. pp. 1-8.

[14] Chiang SJ, Yen CY, Chang KT. A multi module parallelable series-connected PWM voltage regulator. IEEE T Ind Electron 2001; 48: 506–516.

[15] Xiaoxiao Y, Khambadkone AM, Huanhuan W, Terence S. Control of parallel-connected power converters for low-voltage microgrid—Part I: A hybrid control architecture. IEEE T Power Electron 2010; 25: 2962-2970.

[16] Stevenson WD. Elements of Power System Analysis. Singapore: McGraw-Hill International Editions, 1982.

[17] Harris MB, Kelley AW, Rhode JP, Baran ME. Instrumentation for measurement of line impedance. In: Proceedings of the IEEE Applied Power Electronics Conference; 1994. New York, NY, USA: IEEE. pp. 887-893.

[18] Gasperi ML, Jensen DL, Rollay DT. Method for AC powerline impedance measurement. IEEE T Ind Appl 2008; 44: 1034-1037.